Passive UHF RFID Antennas for Sensing Applications: Principles, Methods, and Classifications

C. Occhiuzzi, S. Caizzone, and G. Marrocco

Universita' di Roma "Tor Vergata"
Via del Politecnico, 1, 00133 Roma, Italy
Tel: (+39) 06 72597418; Fax: (+39) 06 72597460;
E-mail: marrocco@disp.uniroma2.it; occhiuzzi@disp.uniroma2.it; stefano.caizzone@gmail.com

Abstract

UHF passive radio-frequency identification technology is rapidly evolving from simple labeling of things to wireless pervasive sensing. A remarkable number of scientific papers demonstrate that objects in principle can have their physical properties be remotely tracked and monitored all along their life cycle. The key background is a new paradigm of antenna design that merges together the conventional communication issues with more-specific requirements about sensitivity to time-varying boundary conditions. This paper presents a unified review of the state of the art of the tag-as-sensor problem. Particular care is taken to formalize the measurement indicators and the communication and sensing tradeoff, with the purpose to provide a first knowledge base for facing a large variety of emerging sensing applications.

Keywords: RFID; antennas; sensors; Internet of Things

1. Introduction

Radio-rrequency identification (RFID) is nowadays a well-assessed technology for tracking goods and for tracing procedures, with several advantages over barcode systems [1]. More-complex applications are currently being researched worldwide in many university laboratories, concerning sensing, localization, other frequency bands, new materials, and more-efficient communication protocols. The sensing capabilities offered by passive RFID tags in the UHF bands are perhaps the most exciting research trend, with great applicability to the emerging paradigm of the Internet of Things [2]. A "swarm" [3] of low-cost tiny interconnected sensors, interacting with the nearby environment, will enable an augmented perception of the reality, stimulating improvements in *well-being* as well as completely new services. For such forthcoming applications, spatial granularity is a key concept [4]. Because of their intended massive use, sensors do not need to be extremely sophisticated or precise. *However, at the same time*, they must satisfy low-cost requirements in order to be deployed at finer granularity than active precise wireless systems. The ultimate goal is to design "smart dust motes" [5], i.e., autonomous sensing, computing, and communication systems small enough to be easily "dispersed in the environment." In order to enable such a vision, passive UHF RFID technology can play a strategic role, thanks to its low-cost, wireless, and "sensing-friendly" capabilities.

The use of an antenna as part of a passive sensor is not new, and occurred much before the appearance of RFID microchips. In the late 1940s, the Russian inventor, Leon Theremin [6], developed one of the first covert listening devices (the "bug"). This used a capacitor microphone connected to an antenna (Figure 1) to transmit away – through reflection of an interrogating carrier – the audio signals captured in nearby environments.

On approaching our times, the unique feature of RFID microchip modulators further adds a completely new sensing possibility. It does this by taking into consideration that RFID tags are tiny computers of increasing performance, with tiny low-power radios that merge together both digital (the microchip and binary data generation) and analog (antennas and propagation phenomenology) features. Data transmitted back to the reader during the interrogation protocol are digitally encoded, but the strength of the backscattered power is governed in an analog manner by the interaction with nearby objects, by the propagation modality, and even by the mutual

 ISSN 1045-9243/2012/$26 ©2013 IEEE

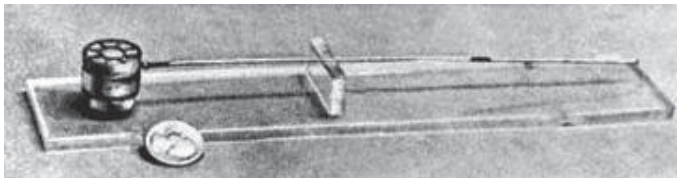

Figure 1. Theremin's bug (1945), the first passive radio sensor converting voice pressure into a modulation of the radar cross section of a wire antenna through a capacitor microphone.

position and orientation among the reader and the tags. This fact poses the basis for a different sensing modality, wherein the captured data can even be collected by a "sensor-less" tag, just by exploiting the physics of the RFID response.

In the last three to five years, a remarkable number of scientific papers have demonstrated – at different levels of maturity and for different applications – that passive RFID sensing can be affordable with the available manufacturing technology. However, an important effort is still required to fully understand and to manage the physics of RFID sensing, and evolve from isolated laboratory experiments to first stable and self-consistent products. In particular, a systematization of phenomena, metrics, and system parameters is of prominent relevance to provide tools for evaluating the true performance of the tag as a sensor, and to make comparisons among different implementations.

The present work follows the style of a previous paper of the same authors [7], wherein the basic design options for general-purpose UHF tags were described in a unitary way. Starting from the more-recent contribution in [8], the present work tries to systematize the different applications of UHF RFID *antennas for passive sensors*. Particular care is taken to clarify the relationships and constraints for communication and sensing, and to introduce performance parameters for general application.

The paper is organized as follows. Section 2 introduces the parameters that can be measured by RFID readers, and some possible metrics relating measurements to the process under observation. Section 3 discusses the cohabitation between the performance of a tag as a sensor and the constraints over the required reading distance. An overall communication-sensing nomogram is introduced. Section 4 describes the class of *bare* tags, the sensing capability of which is only related to the natural sensitivity of an antenna to time-variant boundary conditions. The kinds of *loaded* tags, including specific chemical and mechanical sensor loads, are analyzed in Section 5. Section 6 finally shows the achievable resolution of the whole tag-reader system, depending on the kind of metrics used. To complete the analysis, a quick overview of the new emerging sensing paradigms is finally given in Section 6. Theoretical discussions and classifications are corroborated by many examples taken from recent scientific literature.

2. Measurable Data and Metrics

An RFID system comprises two components. The first is the remote transponder or *tag*, including an antenna and a microchip transmitter (*IC*), located on the object to be identified. The second is the local querying system or *reader*, which can collect data transmitted from the tag (Figure 2), eventually performing a first processing function. Various kinds of data – and, first of all, a unique identification code (ID) – can be wirelessly transferred to the reader by means of radio-frequency electromagnetic signals.

The tags can be *passive*, harvesting energy from the interrogating system; *semi-active*, when a battery is included to only feed the sensors; or *fully active*, where a local source directly feeds a microcontroller as well as the transmitting radio. This work is focused on passive systems, which may have an almost unlimited life and very low cost. Among the actual options, the most-attractive standard is the UHF band (frequency allocations and maximum power emission are given in Table 1), which, in principle, promises activation ranges up to 10 m.

In *passive* technology, at the beginning of the reader-to-tag communication protocol [9], the reader first activates the tag, which is placed over a target object. This is done by sending

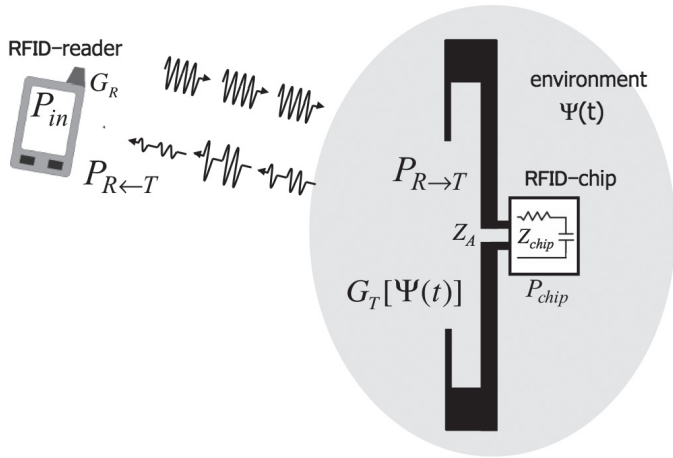

Figure 2. A sketch of the RFID sensing system. A reader interrogates the tag, the behavior of which is influenced by a changing physical feature, Ψ.

Table 1. Worldwide UHF band and power limitations.

Country	Band (MHz)	Max EIRP (W)
Europe	866-869	3.2
USA	902-928	4.0
Japan	950-956	4.0

a continuous wave, which, by charging an internal capacitor, provides the required energy to perform actions. During this *listening mode*, the microchip exhibits an input impedance $Z_{chip} = R_{chip} + jX_{chip}$, with X_{chip} being capacitive. The antenna's impedance, $Z_A = R_A + jX_A$, has to be matched to Z_{chip} ($Z_A = Z_{chip}^*$) for maximum power transfer (a comprehensive review of the techniques for matching the antenna with the chip was provided in [7]). During the next steps of the communication, the tag receives commands from the reader, and finally sends back the data through a *back-scattered modulation* of the continuous wave provided by the reader, itself. In this case, the tag's IC acts as a programmable switching device between a low impedance and a high impedance, thus modifying the reflectivity of the responding tag, and hence the strength of the reflected power.

2.1 Measurable Parameters

In order for a tag to monitor physical parameters, a sensing functionality needs to be added, either physically or just logically. Before going into a particular sensing problem, it is hence useful to introduce the basic RFID electromagnetic parameters suitable to sensing purposes. A single-chip configuration is considered throughout the paper, but the same ideas may nonetheless be extended to the multi-chip systems recently introduced in [10-12].

Let us denote with $\Psi(t)$ a local physical, chemical, or geometrical parameter of the environment surrounding the tag (the *Sensor-tag*, hereafter the *S-tag*), which has to be monitored by the RFID platform. According to the specific applications, Ψ could be the presence of gases and chemical species able to react with the sensitive materials integrated into the antenna; a physical stimulus, e.g., an acceleration able to affect a discrete sensor loading the RFID tag; a shape factor of a biological process; the temperature of the environment; or the local effective permittivity "sensed" by the tag's antenna.

Sensing indicators can be easily derived from data measurable by the reader. For this purpose, the equations of a two-way reader-tag link [13] need to be rewritten, making explicit the dependence on the variation of local parameters [8]. Under the simplifying hypothesis of free-space interactions, the power collected at the microchip, Equation (1), and the power backscattered by the tag toward the reader, Equation (2), and collected by it, are the following:

$$P_{R\rightarrow T}[\Psi] = \left(\frac{\lambda_0}{4\pi d}\right)^2 P_{in} G_R(\theta,\phi) G_T[\Psi](\theta,\phi)\tau[\Psi]\eta_p, \quad (1)$$

$$P_{R\leftarrow T}[\Psi] = \frac{1}{4\pi}\left(\frac{\lambda_0}{4\pi d^2}\right)^2 P_{in} G_R^2(\theta,\phi)\eta_p^2 rcs_T[\Psi(\theta,\phi)], \quad (2)$$

where d is the reader-tag distance, G_R is the gain of the reader's antenna, and $G_T[\Psi]$ is the gain of the tag's antenna at the specific realization of the process. P_{in} is the power entering the reader's antenna, η_p is the polarization mismatch between the reader and the tag, and $\tau[\Psi]$ is the power transmission coefficient of the tag:

$$\tau[\Psi] = \frac{4R_{chip}R_a[\Psi]}{\left|Z_{chip} + Z_a[\Psi]\right|^2}. \quad (3)$$

Finally, rcs_T is the tag's radar cross section, related to the modulation impedance, Z_{mod}, of the microchip for encoding the low and high digital states:

$$rcs_T[\Psi] = \frac{\lambda_0^2}{4\pi} G_T^2[\Psi](\theta,\phi)\left(\frac{2R_a[\Psi]}{\left|Z_{mod} + Z_a[\Psi]\right|}\right)^2. \quad (4)$$

The backscattered power, $P_{R\leftarrow T}$, is measurable (Figure 3a) by the reader in terms of the received signal-strength indicator (RSSI), here assumed to correspond [13, 14] to the binary modulating state having $Z_{mod} = Z_{chip}$.

Another parameter that can be measured by the reader is the *turn-on power* $P_{in}^{to}[\Psi]$, e.g., the minimum input power, P_{in}, through the reader's antenna forcing the tag to respond (Figure 3b). It can be derived from Equation (1) by considering $P_{R\rightarrow T} = P_{chip}$, with the latter being the microchip's sensitivity:

$$P_{in}^{to}[\Psi] = \left(\frac{\lambda_0}{4\pi d}\right)^{-2} \frac{P_{chip}}{G_R(\theta,\phi)\eta_p G_T[\Psi](\theta,\phi)\tau[\Psi]}. \quad (5)$$

From turn-on measurement, it is possible to extract by proper calibration [15] the *realized gain* of the tag, $\hat{G}_T = G_T\tau$, e.g., the gain of the tag scaled by the mismatch to the IC.

Finally, forward (Equation (1)) and backward (Equation (2)) powers may be combined at the turn-on condition with the purpose of dropping out the influences of the distance and of the reader's and tag's gains and orientations [11, 12]. A non-dimensional indicator (Figure 3c), denoted as the *Analog Identifier* (AID), can hence be introduced:

$$AID[\Psi] = \frac{P_{chip}}{\sqrt{P_{R\leftarrow T}[\Psi]P_{in}^{to}[\Psi]}} = \frac{2R_{chip}}{\left|Z_{chip} + Z_a[\Psi]\right|}. \quad (6)$$

The AID only depends on the antenna's impedance. It thus appears useful when the interrogation setup changes (position and orientation) in successive measurements, since it is immune to the interrogation modalities.

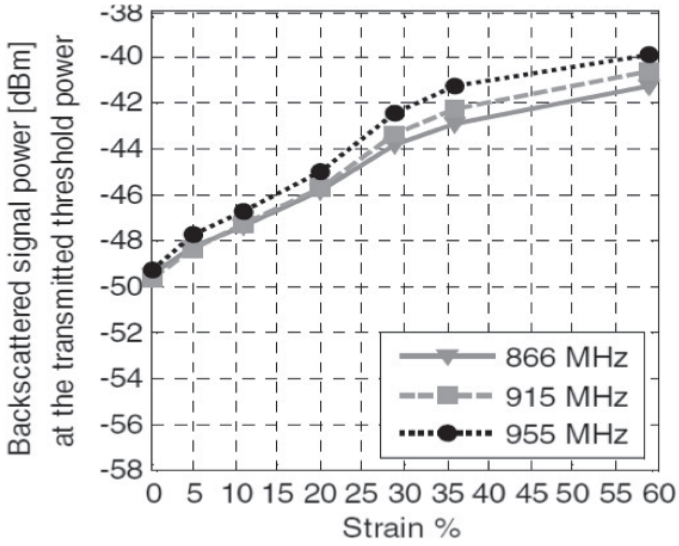

Figure 3a. Examples of measured sensing indicators: back-scattered power as a function of strain [17]

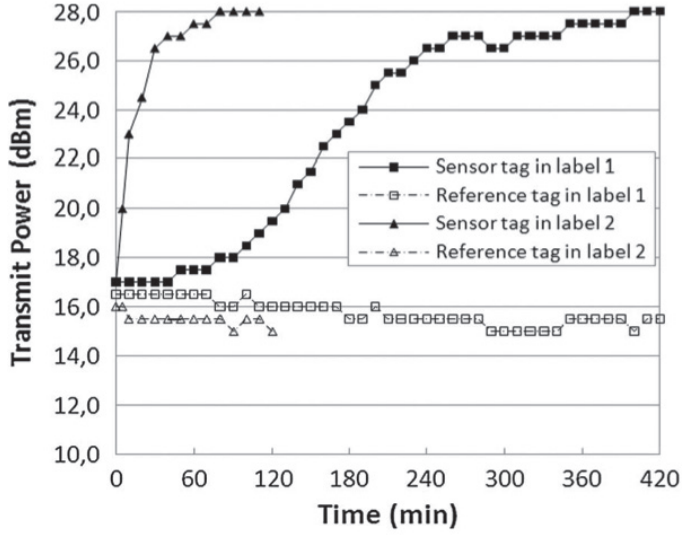

Figure 3b. Examples of measured sensing indicators: turn-power as a function of humidity [18].

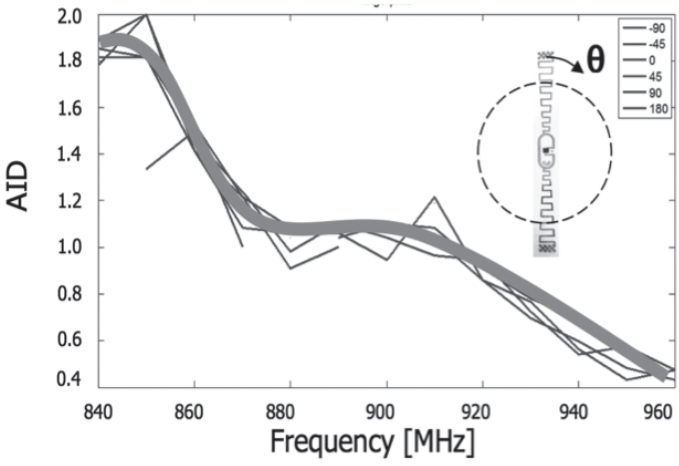

Figure 3c. Examples of measured sensing indicators: an analog identifier measured at different observation angles [12].

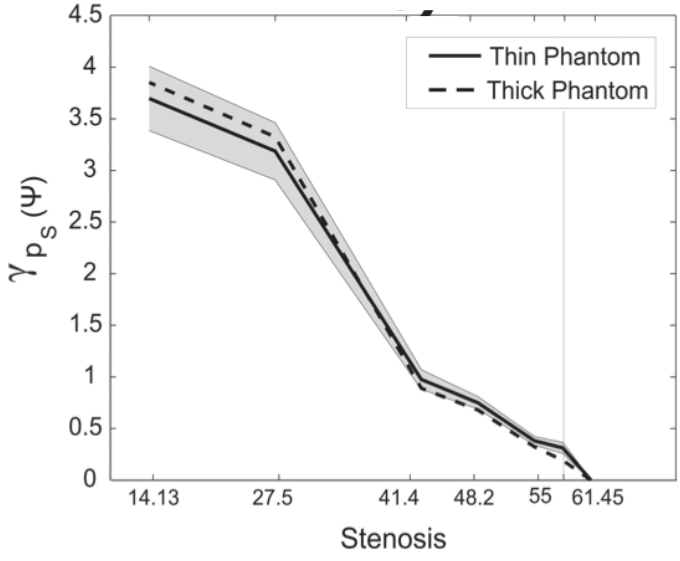

Figure 3d. Examples of measured sensing indicators: integral metrics: scale factor [19].

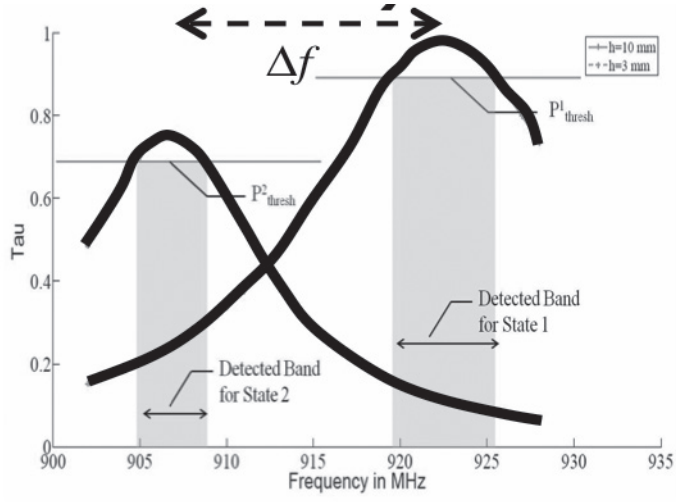

Figure 3e. Examples of measured sensing indicators: integral metrics: frequency shift [20].

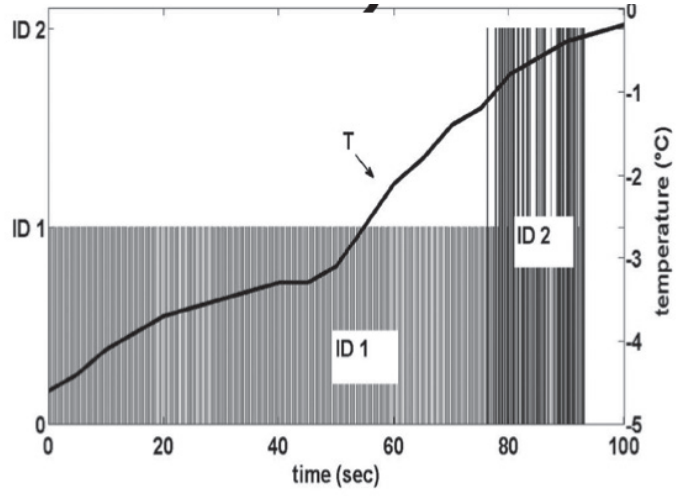

Figure 3f. Examples of measured sensing indicators: binary detection of temperature threshold [21].

 ISSN 1045-9243/2012/$26 ©2013 IEEE

Other kinds of direct metrics may be defined, just like the differential reflection coefficient in [16], which even accounts for the different responses of the antenna in the two modulating states.

2.2 Sensing Metrics

The indicators in Equations (2), (5), and (6), may be used as *data inversion curves* between the measured data and the evolution, $\Psi(t)$, of the process:

$$\{AID, P_{in}^{to}, P_{T\to R}\} \leftrightarrow \Psi(t), \tag{7}$$

It could be useful to normalize each indicator by its value in a particular reference state, say Ψ_0, for instance collected at the time of the tag's placement into the environment to be monitored. The normalized parameters are hereafter generically indicated with $\xi[\Psi]$. They can be collected at a fixed frequency, or instead within the whole RFID band to provide integral metrics suitable for capturing macroscopic variations of the S-tag response over frequency, such as the detuning and the attenuation or magnification of the response (Figures 3d and 3e). The *frequency shift*, e.g., the frequency correlation distance, Δf, between $\xi[\Psi](f)$ and the initial response, $\xi[\Psi_0](f)$,

$$\Delta f[\Psi]: \int_{f_1}^{f_2} \xi[\Psi]_0(f)\,\xi[\Psi](f+\Delta f)\,df \text{ is maximum} \tag{8}$$

gives a measure of the change of the antenna's resonance due to the evolving chemical-physical process. The *scale factor*,

$$\gamma[\Psi] = \frac{\int_{f_1}^{f_2} \left|\xi[\Psi](f-\Delta f) - \xi[\Psi_0](f)\right| df}{\int_{f_1}^{f_2} \left|\xi[\Psi_0](f)\right| df}, \tag{9}$$

instead describes the overall attenuation/amplification of the S-tag's response. These two indicators look particularly useful in those countries wherein the available bandwidth for UHF RFID is significant, such as the USA. Their application is less effective in Europe, due to the very modest allowed bandwidth.

As for usual sensors, the response of the S-tag can be quantified by the *dynamic range*, e.g., the overall change of the measured parameters between the extreme interesting realizations of the process, Ψ_{min}, Ψ_{max}, conveniently expressed in decibels:

$$\Delta\xi = \left|\xi[\Psi_{max}] - \xi[\Psi_{min}]\right|_{dB}, \tag{10}$$

and by means of the *sensitivity*,

$$S[\xi] = \frac{\partial \xi[\Psi]}{\partial \Psi}. \tag{11}$$

If the S-tag's response is approximately linear in the useful range of the process, then

$$S[\xi] \simeq \frac{\Delta\xi}{\Psi_{max} - \Psi_{min}}. \tag{12}$$

The sensitivity and the dynamic range of the system are thus strictly connected to the antenna's features, in particular to its quality factor, and definitely to its bandwidth. On considering the whole reader/S-tag system, the overall performance parameter is the *resolution*, which accounts also for the discretization of the reader's signals. This topic is of prominent importance for the true real applicability of S-tags, and will be addressed later on, in a dedicated section.

3. Communication and Sensing Tradeoff

Sensing capabilities are generally achieved at the expense of reading-distance degradation, since the changes of physical/chemical features of the environment are sensed by the passive tag through a deviation from its static gain and/or impedance matching. The true effectiveness of an S-tag thus results from the tradeoff between sensing and communication [19].

3.1 Constraints

Sensing requirements induce a constraint over the dynamic range:

$$\Delta\xi \geq R, \tag{13}$$

with R being the requested span of the measured data. Preserving a useful reading range in all the states of the process instead means enforcing a condition over the minimum turn-on power (see Figure 4):

$$P_{in}^{to}(\Psi) \leq p, \quad \Psi_{min} \leq \Psi \leq \Psi_{max}. \tag{14}$$

The power bound, p, has to comply with the local regulations (Table 1), and with the true available power for fixed or hand-held readers. Having selected the reader-tag distance, from Equation (5) such a constraint will enforce the minimum allowed value for the realized gain all along the process:

$$G_T(\Psi)\tau(\Psi) \geq g \text{ for } \Psi_{min} \leq \Psi \leq \Psi_{max}. \tag{15}$$

It is worth noticing that an S-tag can be turned into a detector of a particular state, Ψ_k, of the process if the antenna is really narrowband, so that the condition of Equation (14) holds just in the region closely surrounding Ψ_k, e.g.,

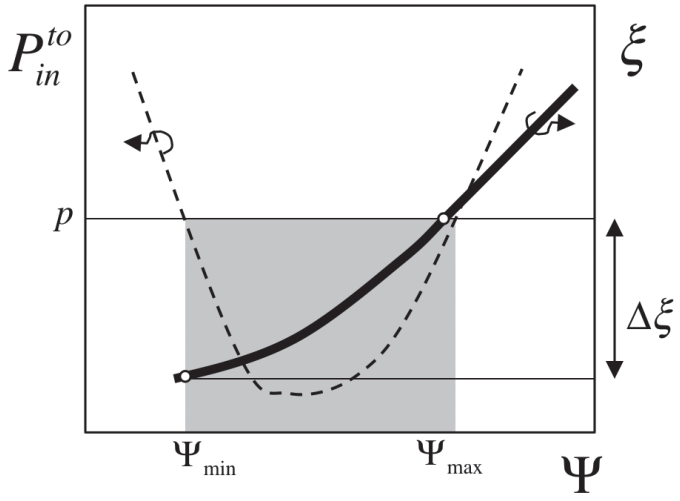

Figure 4. The pictorial relationship between the maximum sensing dynamic range, $\Delta\xi$, of an S-tag, and the constraints over the maximum power, p, emitted by the reader.

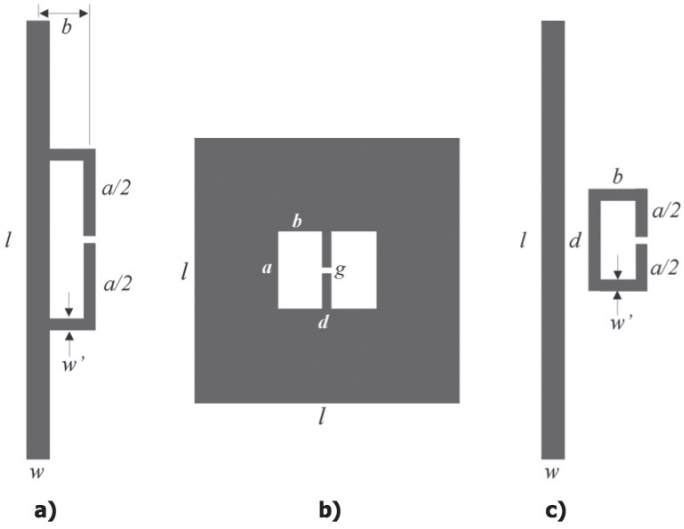

Figure 5. Typical layouts of antenna adapters used to control the impedance response of the tag: (a) T-match, (b) slot-match, (c) loop-match.

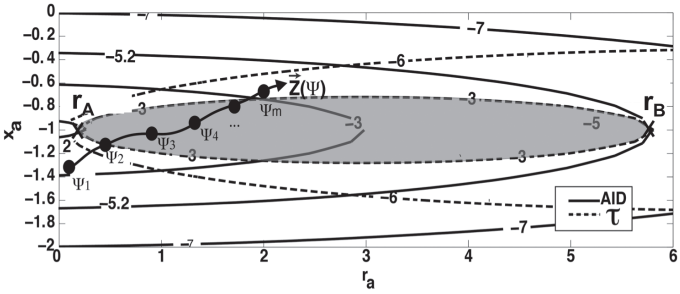

Figure 6. Iso-lines of constant AID and τ on the normalized antenna-impedance plane, for an IC's quality factor of $Q=10$. The area corresponding to $\tau_{min}=-3$ dB is in gray. The curve $\vec{Z}[\Psi]=r_a(\Psi)\hat{i}+x_a(\Psi)\hat{j}$ indicates a possible variation of the antenna's impedance all along the process in evolution.

$|\Psi_{max}-\Psi_{min}|\to 0$ in Figure 4. A discrete set of events of the process may hence be recognized by using a multiplicity of tags or a single multi-port tag (Figure 3f), with different impedance-matching conditions, as described in [10]. Each event Ψ_k to be recognized is accordingly linked to the ID_k of the microchip, which has scavenged enough power to interact with the reader ($P_{k,in}^{to}(\Psi_k)\le p$). In any case, designing S-tags is similar to the design of broadband antennas, or even better, of microwave filters, wherein frequency is replaced by the state of the process.

3.2 Global Tradeoff

In the most general case, the tradeoff between communication and sensing is handled by performing a synthesis of the S-tag's response, $\xi\leftrightarrow\Psi$, by a proper shaping of the geometrical sizes, $\mathbf{A}=\{a_1,..,a_K\}$, of the antenna, as for instance in the case of the profile of meander-line structures [22, 23]. Such a problem can be formalized as the minimization with respect to $\mathbf{A}$ of a multi-objective function [24] such as the following:

$$w_1\sum_{m=1}^{M}\left|\xi\left([\Psi_m,\mathbf{A}]\right)-\xi_m\right|+w_2\sum_{m=1}^{M}\frac{G_0}{G_T\tau[\Psi_m,\mathbf{A}]}, \quad (16)$$

where (Ψ_m,ξ_m), $m=1...M$, are control nodes of the sensing curve, e.g., the desired values of the antenna's response at M realizations of the process; G_0 is the minimum realized gain in order to satisfy Equation (14); and w_1 and w_2 are weights such that $w_1+w_2=1$.

To reduce the degrees of freedom of the problem, the shape of the main radiator may be fixed (for instance, a folded dipole or a PIFA). The tradeoff between communication and sensing is balanced through the shaping of an antenna adapter (Figure 5) in the form of a T-match, a slot match, a loop match, or their variations, as detailed described in [7]. In any case, the above optimization problems can be conveniently solved by a stochastic tool, such as the genetic algorithm [22] or the particle swarm [25].

3.3 $\{\tau[\Psi], AID[\Psi]\}$ Nomogram

Assuming the Analog Identifier in Equation (6) as the measurement metric, the relationship between the communication ($\tau[\Psi]$) and sensing ($AID[\Psi]$) parameters can be visually represented by a specific nomogram [24]. This is useful for estimating the theoretical maximum dynamic range of the tag that can be achievable within the communication constraints in Equation (14). For this purpose, the power-transmission coefficient and the Analog Identifier are expressed in terms of the normalized input impedance of the tag, $r_a=R_A/R_{chip}$,

$x_a = X_a / X_{chip}$, with $Q = |X_{chip}| / R_{chip}$ being the quality factor of the chip:

$$\tau[\Psi] = \frac{4 r_a}{\left|1 + r_a + jQ(1 + x_a)\right|^2}, \tag{17}$$

$$\mathrm{AID}[\Psi] = \frac{2}{\left|1 + r_a + jQ(1 + x_a)\right|^2} = \sqrt{\frac{\tau}{r_a}}. \tag{18}$$

Having fixed Q, a chart of $\{\tau, \mathrm{AID}\}$ isolines is produced in decibels by varying r_a and x_a (Figure 6). Such lines are ellipses, with the major axis over the $x_a = -1$ line, and the eccentricity of which depends on the quality factor, Q, of the microchip. The point $(r_a = 1, x_a = -1)$ corresponds to the *matched state* Ψ_M [19], e.g., the state of the process for which the tag's antenna shows the best matching to the IC. There, $Z_a = Z_{chip}^*$, and $\mathrm{AID} = \tau = 0$ dB.

The τ-AID nomogram does not depend on the particular antenna layout. The variation of the tag's impedance all along the phenomenon evolution can therefore be traced over such a plane by a sequence of couplets, $\{r_a(\Psi_n), x_a(\Psi_n)\}$, describing an oriented curve (Figure 6):

$$\vec{Z}[\Psi] = r_a(\Psi)\hat{i} + x_a(\Psi)\hat{j} \in \mathbb{R}^2. \tag{19}$$

The S-tag will show different sensing and communication behavior all along the process, according to the intercepted isolines.

The communication constrains in Equation (14) or in Equation (15) become conditions over the power-transfer coefficient

$$\tau[\Psi] \geq \frac{g}{G_T(\Psi)} \equiv \tau_{min}. \tag{20}$$

Such a condition defines the region (shadowed in Figure 6) wherein the allowed dynamic range of the tag's response has to be constrained. The maximum variation, ΔAID_{max}, will be given by the AID isolines passed by the extremes $A = (r_A, -1)$, $B = (r_B, -1)$, of the major axis of the $\tau = \tau_{min}$ ellipse. The multi-objective function to be minimized in Equation (16) is hence reduced to a condition on the input-impedance path, $\vec{Z}_m[\Psi]$. The antenna's geometrical parameters, $\mathbf{A}$, have to be engineered in order to force the impedance curve to the straight segment $\vec{Z}_m[\Psi_m, \mathbf{A}] = \overline{AB}$. This means that the best sensing mechanism over the antenna is such as to convert the variation of the process into a change of the only input resistance.

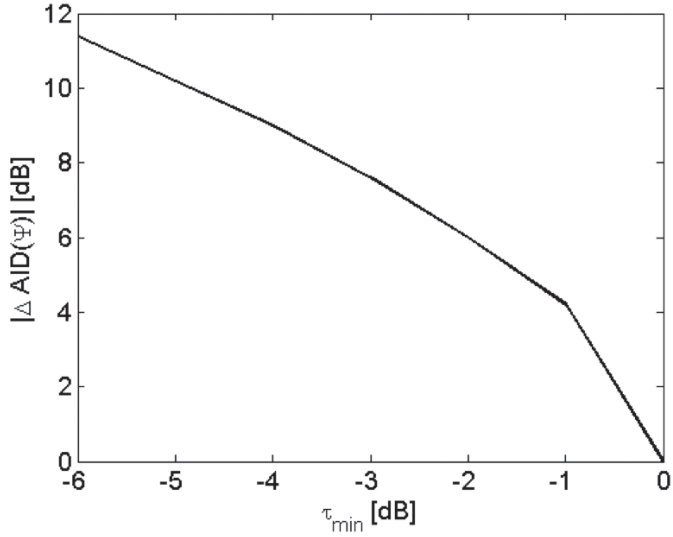

Figure 7. The maximum effective sensing capabilities of the radio sensor for a constant-gain process.

The $\{\tau[\Psi], AID[\Psi]\}$ chart finally provides reference information about the best tradeoff (see Figure 7) between the minimum acceptable reading-range degradation all along the process, e.g., the minimum power-transfer coefficient τ_{min}, and the maximum achievable sensing dynamic range of the measurable indicator $\Delta AID_{max}(\tau_{min})$. For instance, the choice $\tau_{min} = -3$ dB will permit the reading range to not be degraded below 70% of its maximum value corresponding (for example) to the initial (or final) state of the process. Accordingly, the theoretical maximum range of the tag's response will be $\Delta AID = 7.5$ dB.

4. Bare S-Tags

Antennas are inherently sensitive to the change of the background medium. For instance, in the case of a homogeneous space-filling material with parameters $(\mu = \mu_0\mu_r, \varepsilon = \varepsilon_0\varepsilon_r)$, the frequency dependence of the material's input impedance is shifted and scaled with respect to the air according to the Deschamps equation [26]:

$$Z_A(\omega, \varepsilon, \mu) = \sqrt{\frac{\mu_r}{\varepsilon_r}} Z_A\left(\sqrt{\mu_r \varepsilon_r}\,\omega, \varepsilon_0, \mu_0\right). \tag{21}$$

In general, this phenomenon is usually considered to be a limiting factor for RFID, since in order to optimize the tag, the material properties of the item to be tagged need to be known in advance. On the other hand, such performance variations can be interpreted as an intrinsic sensing capability. A modification of the tagged object is globally seen by the tag's antenna as

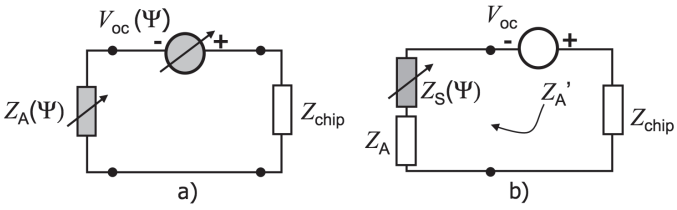

Figure 8. The equivalent receiving circuit for (a) a bare tag for which the antenna impedance and the open-circuit induced voltage become dependent on the phenomenon, Ψ, under observation; and (b) for a tag where the antenna is loaded by a specific lumped sensor placed, for instance, in series with the RFID microchip.

a change of the surrounding equivalent permittivity, which in turn will produce a change of the tag's antenna's impedance and received power (Figure 8a), and ultimately as a variation of the turn-on and backscattered-power indicators. A *self-sensing*, completely sensor-less, passive device is therefore obtained, wherein the *sensor is the antenna and the antenna is the sensor*. The same principle holds when the process under observation induces a deformation of the antenna's shape, as in case of moving surfaces or evolving cracks. However, this sensing mechanism is non-specific, since the sensed data may be only indirectly related to a physical phenomenon under observation.

4.1 Effective Permittivity S-Tags

Figure 9 shows some examples of self-sensing tags, recently proposed for remote observations of liquids, powders, and biological processes. Each tag is documented with the dynamic range achieved and the sensitivity as deduced by the original papers.

- a-b: These are tags used as filling sensors for low-permittivity [15] and high-permittivity processes [27]. The sensing activity can be performed by analyzing the variation of the reverse communication link, e.g., the received signal-strength indicator or, equivalently, the backscattered power of one or more tags, matched at different filling levels. The same approach was used in [28] for measuring urine volume in diapers, primarily targeting infant- and geriatric-care applications. In this work, the dynamic range achieved was $R = 7.8$ dB.

- c: This is an array of six commercially available RFID tags used as discrete detectors of the filling level of a bottle containing water [29]. Since the tags were tuned for operation in air, the ON state, e.g., the ID transmission, occurs when there is no liquid around the tag, while the tag should remain silent when backed by water. By analyzing the specific set of IDs received by the reader, it is possible to retrieve the filling level of the container. The same approach was used in [30] for providing an automatic warning system for running out of injection fluid.

- d: This is a passive RFID bare sensor also used for the detection of water infiltrations into concrete [31]. The presence of water sensibly changes the tag radiation and the matching performance of a tag drowned in the concrete, up to completely detuning it. A binary detection of water is thus proposed by relating the activation of the tag to the absence of water in its surrounding environment. More-accurate and quantitative results may be achieved by considering a customized RFID IC with three modulation states [32].

- e: A passive RFID device is used as a dielectric-property sensor for lightweight concrete. The tag is best matched for a dry condition of the concrete, and experiences mismatch as the specimen exhibits different qualities due to the presence of water [33].

- f: A commercial tag is used to monitor the level in a medical transfusion bag/bottle. The tag is tuned for operation in air, and is therefore strongly detuned when the plastic bag/bottle is filled with transfusion liquid. The communication performance instead increases as the bag becomes empty [34].

- g: A tag is nested into a metallic structure, namely a cardiovascular stent. By adding the RFID IC, it is possible to transform the cardiovascular device into a radio sensor, able to monitor the restenosis process, which induces a change in the properties of the material surrounding the tag [19].

- h: This is a dipole-like tag for the detection of brain edema after surgical treatment for brain cancer [35]. Edema, which here roughly refers to water-imbued brain tissue, modifies the electromagnetic characteristics of the tissues surrounding a 1 cm-long implanted dipole tag, thus affecting the numerically computed two-way RFID link.

4.2 Deformation S-Tags

Some examples of tags recently developed to monitor deformations and displacements are shown in Figure 10, with the corresponding ranges and sensitivities.

- a: This is a dipole-like tag, which can be ink-printed on fabric or on PVC. It can monitor the amount of deformation that it has undergone by monitoring the changes in the backscattered power, thanks to the changes in the effective conductivity of the ink when a strain is applied [17] .

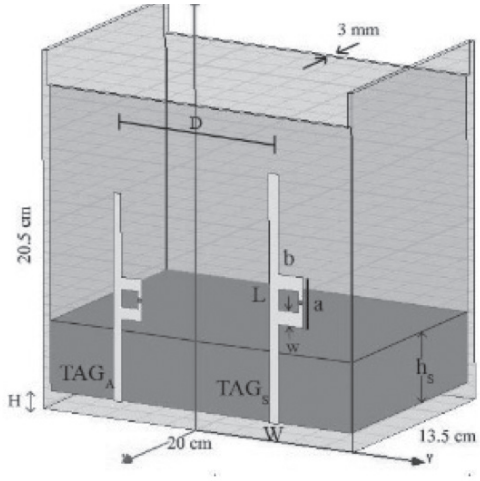

Figure 9a. Examples of effective-permittivity S-tags: a low-permittivity filling-level sensor [15].

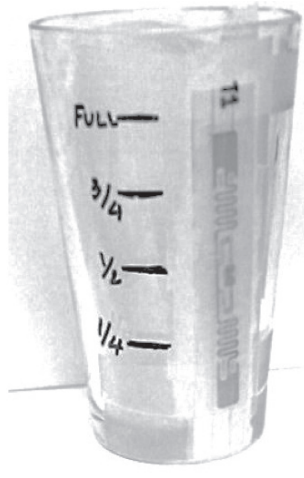

Figure 9b. Examples of effective-permittivity S-tags: a high-permittivity filling-level sensor [27].

Figure 9c. Examples of effective-permittivity S-tags: a high-permittivity discrete filling-level sensor [29].

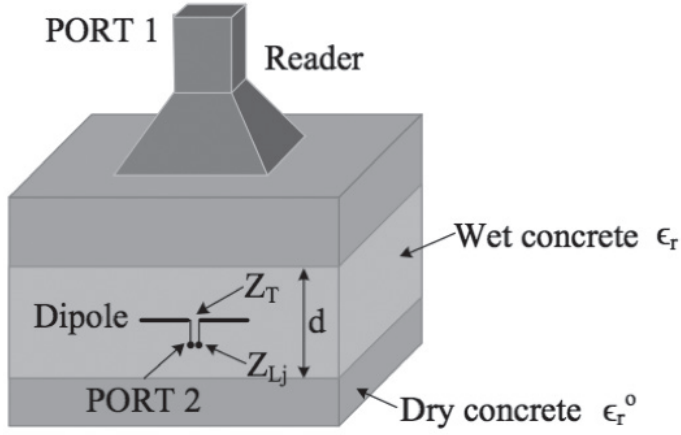

Figure 9d. Examples of effective-permittivity S-tags: a concrete water-infiltration sensor [31].

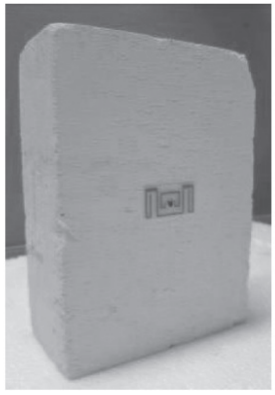

Figure 9e. Examples of effective-permittivity S-tags: a concrete humidity sensor [33].

Figure 9f. Examples of effective-permittivity S-tags: a high-permittivity filling-level sensor [34].

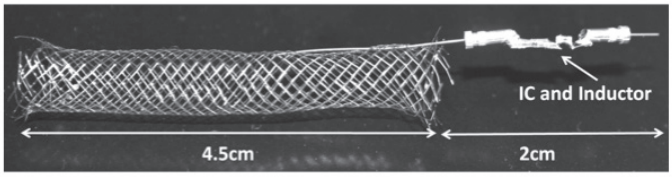

$R\,(P^{TO})=3.5dB$
$R\,(P^{R->T})=6dB$

Figure 9g. Examples of effective-permittivity S-tags, biological process sensors: the STENTag [19].

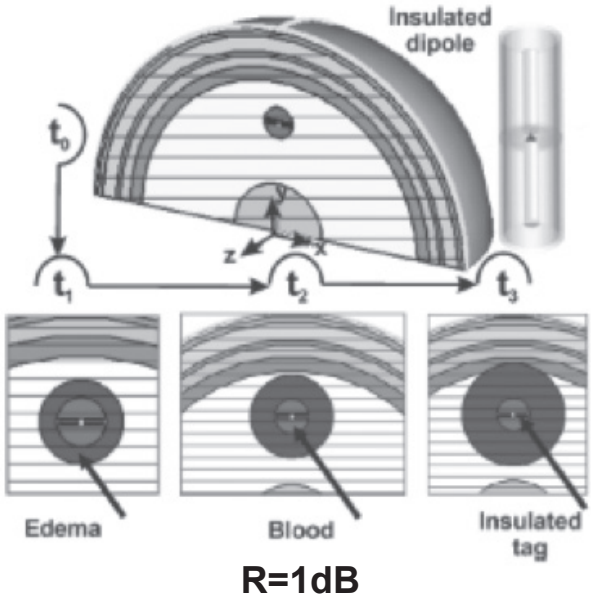

Figure 9h. Examples of effective-permittivity S-tags, biological process sensors: cerebral edema monitoring [35].

- b: This is a meander-line antenna, designed to monitor strains. By applying an elongation, its shape will turn from a tightly-twisted meander to a zigzag dipole, thus altering the antenna's properties, such as the ratio of the actual backscattered power to the backscattered power measured during the steady state [36].

- c: This is a displacement sensor, obtained by exploiting the detuning characteristics of a metal plate behind a dipole-like tag. The metal plate is attached to the structural beam to be monitored, and the RFID tag is placed in proximity to the metal plate, facing the RFID reader. When loading occurs on the beam, a degradation of RFID tag performance is recordable at the reader, because of the destructive effect of the metal plane, now closer to the tag [37].

- d: This is a strain and crack sensor, realized by means of a folded patch antenna. The application of a tensile strain on the antenna results in a frequency shift of the turn-on power, due to a longer electrical path [38].

- e: This is a method for motion capture by using passive UHF linearly polarized tags properly placed on human-body segments. Dual-polarized reader antennas are used to estimate the inclination of each tag, based on the polarizations of the tag's responses [39].

5. Loaded S-Tags

A more effective way to retrieve specific sensing data is to provide the tag with a "real" sensor. This could be either lumped into a device [40, 41], connected in some part of the tag's antenna (Figure 8b) [42-44], or instead distributed all over the antenna's surface, for instance, as a chemical-receptor painting [45]. The sensor is hence considered as a lumped or distributed impedance loading, $Z_S(\Psi)$, on the tag's antenna. The variation of $Z_S(\Psi)$ caused by the change of the environment will accordingly produce a change of the tag's gain and impedance, wirelessly detectable by measurement of the previously described indicators.

The design of such a class of S-tags can be performed by the same approach as in Equation (16) with the additional degrees of freedom of sensor displacement over the antenna. It is worth noticing that this problem is similar to the design of loaded antennas – very popular in HF naval and vehicular communications – to achieve broadband and multi-band communications. In that context, the position and number of loads (RLC circuits, called "traps") are optimized by using a multi-port network representation of the antenna (see [46] for more details). The same idea could in principle also be applied to S-tag design. In the following sections, many examples are given, grouped according to the type of impedance loading.

5.1 Chemical Loading

Different kinds of S-tags loaded by chemical compounds are shown in Figure 11.

- a: This is a moisture sensor loaded by a chemical species [47]. In this case, the sensitive material is simply blotting paper, eventually doped with NaCl (salt), covering an RFID patch-like tag. Since the paper absorbs water, the radiation performance of the tag sensibly degrades, thus producing appreciable variations of the tag's response link.

- b: This is a loop-driven flat dipole, doped with carbon nano structures (CNT) [45]. It is able to sense the presence of ammonia in the environment, thanks to the absorbing property of the carbon nano

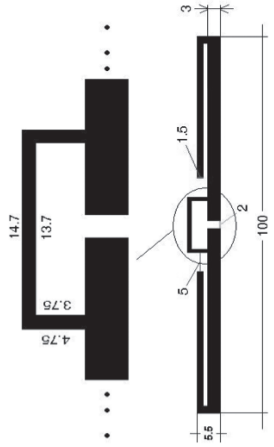

$$R(PVC) = R(fabric) = 10dB$$
$$S(PVC) = 0.16dB/(strain\ \ \%)$$
$$S(fabric) = 0.32dB/(strain\ \ \%)$$

Figure 10a. Examples of S-tags suitable for sensing geometrical changes of objects: an ink-printed stretchable folded dipole [17].

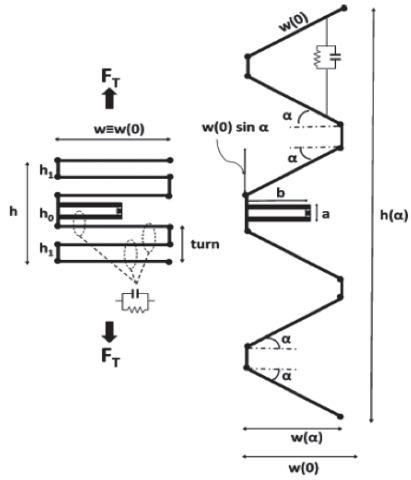

$$R = 10dB$$
$$S = -0.5dB/(strain\ \ \%)$$

Figure 10b. Examples of S-tags suitable for sensing geometrical changes of objects: a flexible meander-line antenna [36].

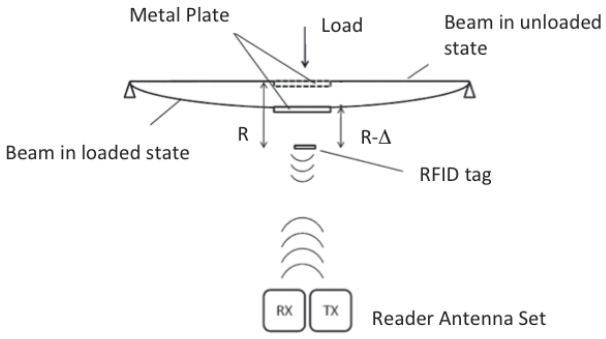

$$R = 13dB$$
$$S = -0.35dB/mm$$

Figure 10c. Examples of S-tags suitable for sensing geometrical changes of objects: proximity detuning by moving conductors [37].

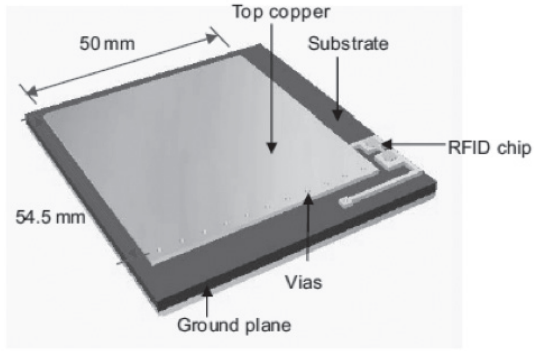

$$S = -5.5MHz/(strain\ \ \%)$$

Figure 10d. Examples of S-tags suitable for sensing geometrical changes of objects: a deformable patch [38].

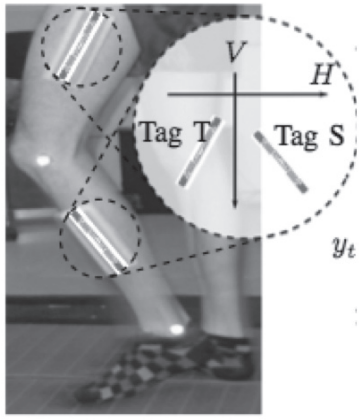

$$R = 19dB$$

Figure 10e. Examples of S-tags suitable for sensing geometrical changes of objects: a motion-capture method [39].

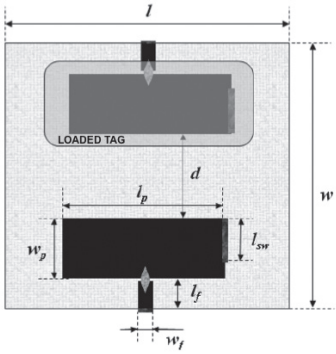

$$\Delta RH = 50\%$$
$$R = 12dB$$
$$S_{low\,RH} = 0.13dB/\%RH$$
$$S_{high\,RH} = 0.3dB/\%RH$$

Figure 11a. Examples of chemically loaded tags: a moisture sensor integrating blotting paper [47].

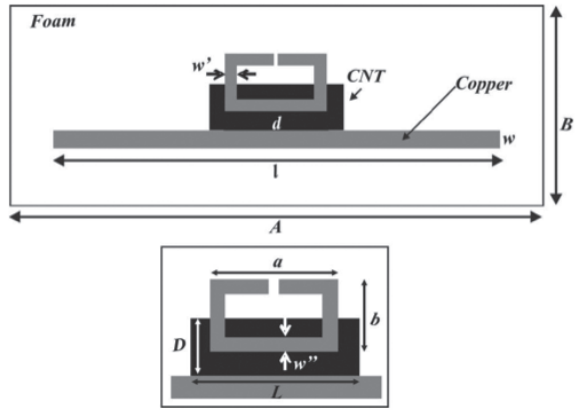

$$R = 2dB$$

Figure 11b. Examples of chemically loaded tags: an ammonia sensor integrating carbon nanotubes [45].

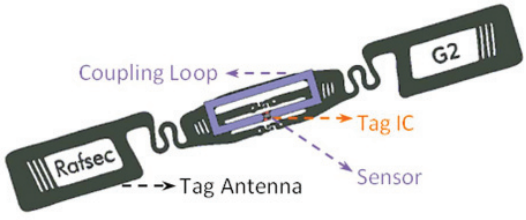

$$\Delta RH \approx 30\%$$
$$R = 13dB$$

Figure 11c. Examples of chemically loaded tags: a humidity sensor integrating a resistive printed load [18].

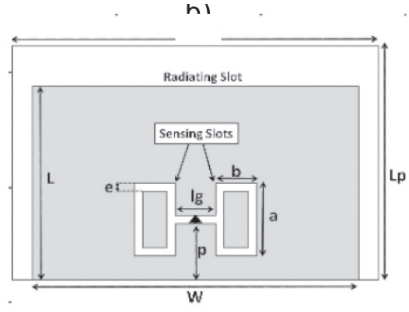

$$\Delta RH = 50\%$$
$$R = 8dB$$
$$S_{low\,RH} = 0.18dB/\%RH$$
$$S_{high\,RH} = 0.13dB/\%RH$$

Figure 11d. Examples of chemically loaded tags: a humidity sensor integrating PEDOT:PSS [48].

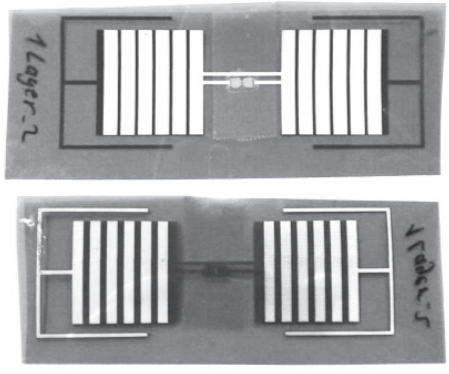

$$\Delta RH \approx 100\%$$
$$S = 171KHz/\%RH$$

Figure 11e. Examples of chemically loaded tags: a moisture sensor with sensitive dielectrics [49].

$$\Delta T = 66°C$$
$$S = (729.5 \pm 7.5)KHz/°C$$

Figure 11f. Examples of chemically loaded tags: a temperature sensor integrating distilled water [50].

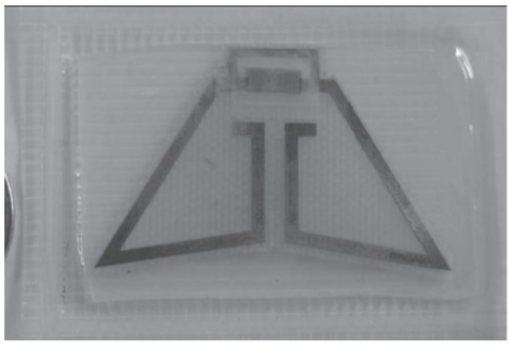

$$\Delta T = 40°C$$

$$S = 0.1dB/°C$$

Figure 11g. Examples of chemically loaded tags: a temperature sensor on paraffin wax [51].

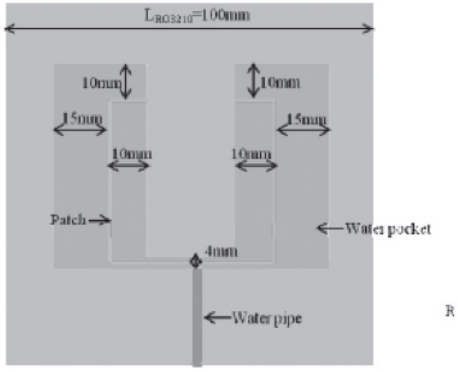

$$\Delta T = 30°C$$

$$S = 0.6MHz/°C$$

Figure 11h. Examples of chemically loaded tags: a temperature sensor integrating a water pocket [52].

structure material deposited between the matching loop and the dipole. Changes in the properties of the carbon nano structures will reflect in mismatch and gain variations, readable through turn-on and backscattered power measurements.

- c: This is a tag connected to a one-way moisture sensor by means of a coupling loop. The printed sensor operates as a write-once-read-many (WORM) resistive memory device, as it permanently changes its resistance from about 10k Ω to 10 Ω after exposure to moisture or water [18].

- d: This is a wearable tag [53], comprising a folded planar structure over a Teflon substrate 4 mm thick, provided with a radiating edge and a sensing H-shaped slot wherein gas-sensitive polymers can be spread. The material used in this work was the commercial species Clevios PH 500, a dispersion for conductive coatings with PEDOT and PSS. Like other polymers containing sulfonic acid groups, PEDOT:PSS is strongly hygroscopic. It takes up moisture when handled under ambient conditions, and consequently changes the tag's radiation performance [48].

- e: This is a printed dipole loaded by distributed capacitors [49] for humidity sensing. The capacitors convert the permittivity variations of the substrate into a change in the antenna's impedance, remotely detectable through the frequency shift of the turn-on power measurements.

- f: This is a printed T-matched dipole-like tag, loaded by distilled water encased within a plastic container, and placed in close proximity to the impedance-matching network [50]. The tag is capable of temperature monitoring. The varying electrical properties of the water alter the operation of the RFID tag itself throughout the impedance-matching network. The turn-on power of the sensor experiences a frequency shift when measured at different temperatures.

- g: This is a small tag printed on top of a multilayer substrate, including paraffin wax for temperature monitoring. As the temperature increases, the electrical properties of paraffin wax change, leading to mismatched operation for the tag, and hence resulting in temperature-sensing capabilities through turn-on measurements [51].

- h: This is a patch-like tag printed on a multilayer substrate, including a small water pocket. Thanks to the change of the water's properties, the resonance of the tag shifts away along with temperature. It is possible to monitor temperature variations while keeping a good reading range [52].

5.2 Mechanical Switch Loading

Tags integrated with process-controlled switches have been mainly employed for discrete sensing (Figure 12), e.g., with the purpose of detecting and transmitting the occurrence of one or more specific states by ID modulation.

- a: This is a two-chip tag integrated with a temperature switch. One port of the tag is always active (i.e., it can be read at any temperature, giving the information of the tag's existence), while the other port is shunted with a shape-memory alloy (SMA) wire, which changes state at a given temperature, hence inhibiting or not inhibiting the transmission of the code of the second chip [42].

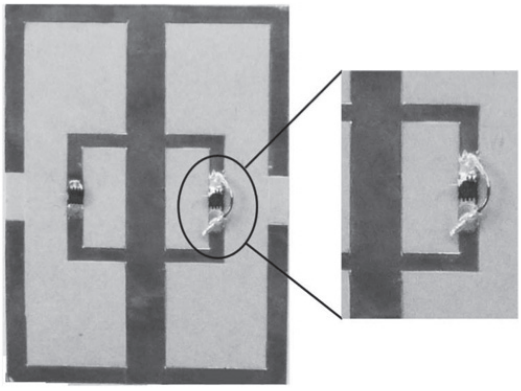

Temperature switch

Figure 12a. Examples of S-tags loaded with mechanical switches: a temperature binary sensor integrating shape-memory alloys [42].

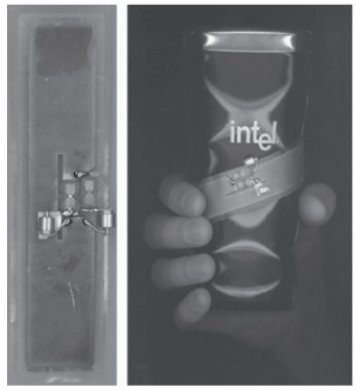

Acceleration switch

Figure 12b. Examples of S-tags loaded with mechanical switches: an acceleration binary sensor integrating an inertial switch [54].

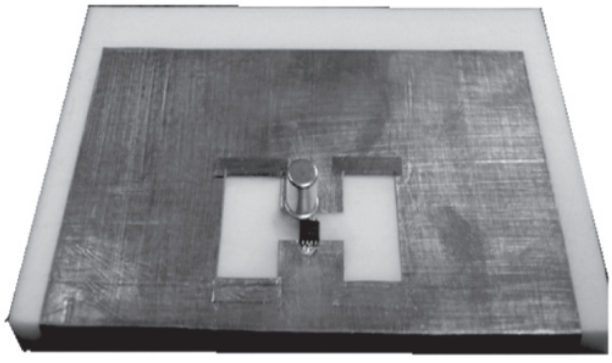

Motion switch

Figure 12c. Examples of S-tags loaded with mechanical switches: a motion binary sensor integrating an inertial switch [53].

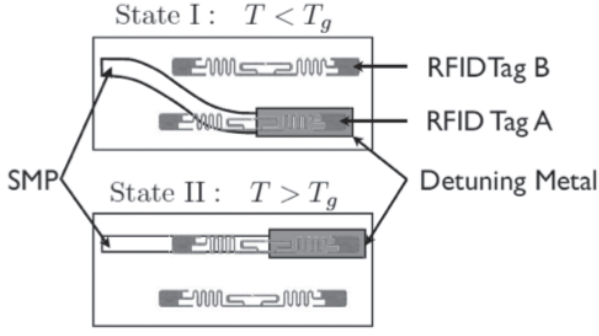

Temperatu re switch

Figure 12d. Examples of S-tags loaded with mechanical switches: a temperature binary sensor integrating a metal plate and shape-memory alloys [55].

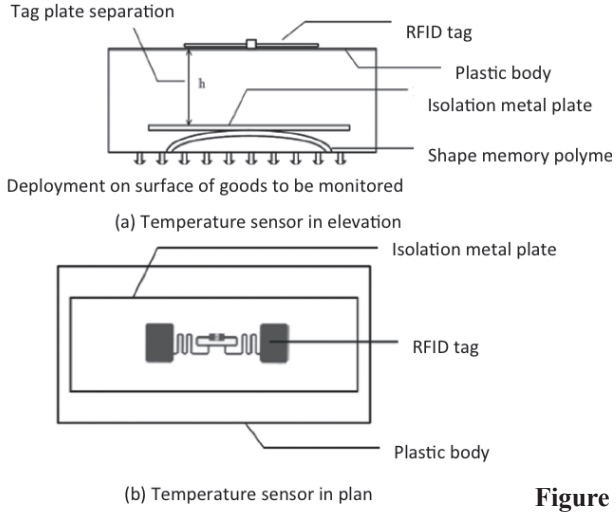

Temperature switch

Figure 12e. Examples of S-tags loaded with mechanical switches: a temperature binary sensor integrating a shape-memory polymer [20].

- b: This is a dipole integrated with a one-bit accelerometer, obtained through the use of two mercury switches, each in series with one chip. By proper mounting of the switches – for instance, in an anti-parallel configuration – it is possible to achieve a "binary-code-shift keying," consisting of ID1 responding when the acceleration is parallel to the first switch, and ID2 responding when acceleration is parallel to switch 2 [54].

- c: This is a wearable slotted-patch antenna, integrated with an inertial omnidirectional switch. In the rest state, this was demonstrated to exhibit a low inductive impedance. If subjected to motion, its impedance fluctuated between an ideal open circuit and the previous value [53].

- d: This is another way to integrate a temperature switch into an RFID tag, by using shape-memory polymers (SMP). Two different commercial tags are used, with a metal plate behind one of them, detuning it. When the temperature overcomes the threshold temperature, a shape-memory polymer moves the metal plate from one tag to the other's background, detuning the tag on the front. In this way, different codes are transmitted to the reader in the two temperature states. A similar sensor was presented in [55]: the actuator this time was an aqueous medium with a desired melting point. When the aqueous medium melted because of over-threshold temperature, the aluminum plate descended because of gravity, detuning the other tag, and thus remotely giving the information about the critical state.

- e: This is a two-state temperature-threshold detector tag [20]. The sensor is capable of relating the violation of a temperature threshold to a shift in the optimal operating frequency at which the tag's antenna is well matched to the tag's IC. The detuning mechanism consists of a metal plate placed behind the tag, the distance of which can be controlled using a temperature-actuated switch, such as, again, a shape-memory polymer (SMP).

For this family of S-Tags including multiple RFID ICs, the design challenge is to control, in a selective way, the responses of a highly-coupled multi-port system, wherein the behavior of each tag is strongly related to the presence and depends on the status of the surrounding tags. The RFID GRID theory in [11, 12] provided all the required equations and procedures to manage multi-chip antennas, which is a problem similar to the design of multi-port-loaded scatterers.

6. Fluctuations and Resolutions

The use of S-tags and readers for sensing measurements requires facing fluctuations and discretization errors (see Figure 13 for an example). The fluctuations are produced by the internal noise of the receiver, due to the limited stability of its components, but also due to the non-stationary communication channel. The fluctuation may be partially reduced by performing a moving-window averaging over a dense set of samples.

The quantization error is instead related to the *resolution of the system*, e.g., the smallest detectable change (hereafter tagged by the symbol "δ") of the quantity that is being measured. Such a variation as $\delta\Psi$ may be written, after Equation (12), as

$$\delta\Psi = \frac{\delta\xi}{S[\xi]}. \tag{22}$$

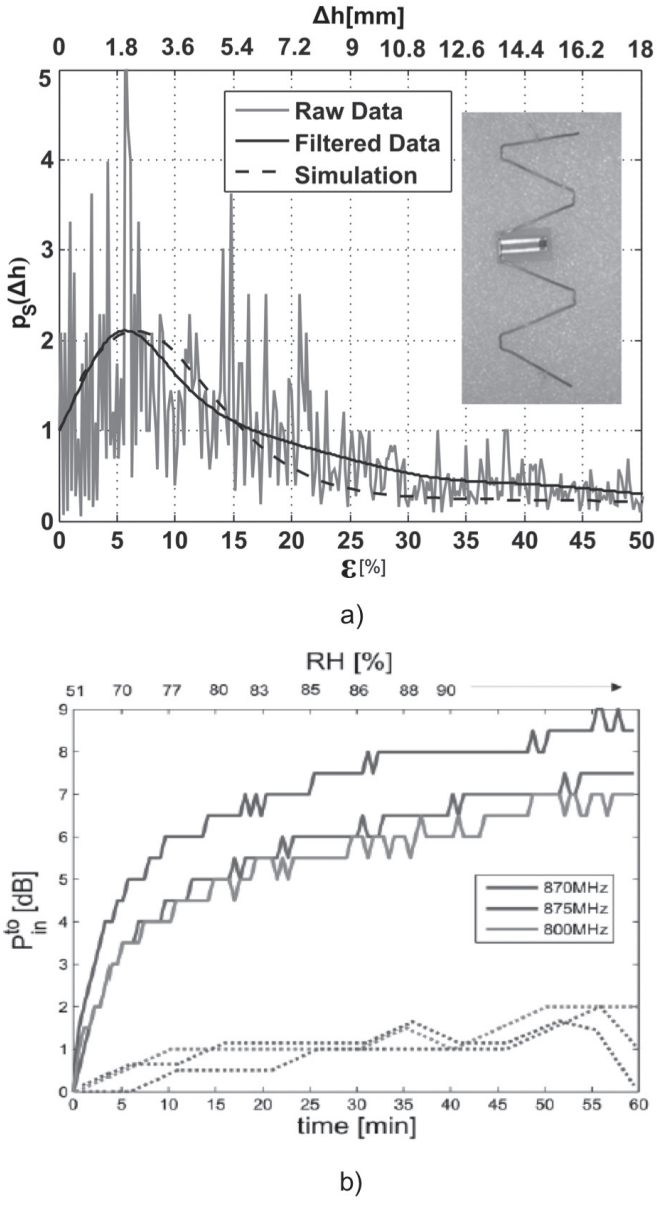

Figure 13. Examples of (a) fluctuations of the received backscattered power (from [36]), and (b) quantization error in the turn-on power (from [48]).

The system resolution, $\delta\Psi$, depends on the sensitivity of the S-Tag, and on intrinsic features of the readers, such as the voltage noise, the random fluctuation of the output signal, and on the quality of the receiving stage.

Finally, the number $n = \Delta\Psi/\delta\Psi$ of observable distinct states of the process between the extreme detectable values $(\Psi_{min}, \Psi_{min} + \Delta\Psi)$ will be therefore expressed in terms of the dynamic range, the S-tag sensitivity and the system resolution as

$$n = \frac{\Delta\xi}{\delta\Psi\, S[\xi]} = \frac{\Delta\xi}{\delta\xi}. \quad (23)$$

The smallest appreciable variation, $\delta\xi$, of the metrics introduced in Section 2 will be analyzed in detail in the following paragraphs.

6.1.1 Backscattered Power ($\xi = P_{R\leftarrow T}$)

Having fixed the power emitted by the reader, then $\delta\xi\big|_{\mathrm{dB}} = \delta P_{R\leftarrow T}\big|_{\mathrm{dB}}$. This parameter depends on the power range of the reader's receiver, and on the analog-to-digital converter (ADC) discretizing the backscattered signal, e.g.,

$$\delta P_{R\leftarrow T}\big|_{\mathrm{dB}} = \frac{range\big|_{\mathrm{dB}}}{2^N - 1}, \quad (24)$$

where N is the number of bits in the analog-to-digital converter. At the time of this writing, commonly available readers provide a received power resolution of the order of from 1 dB down to 0.1 dB.

6.1.2 Turn-On Power ($\xi = P_{in}^{to}$)

The resolution, $\delta P_{in}^{to}\big|_{\mathrm{dB}}$, corresponds to the minimum variation in the output power, δP_{in}^{to}, of the reader that can be controlled by the user. It is fixed by the manufacturer, and it is again of the order of 0.1 dB to 1 dB.

6.1.3 AID ($\xi = AID$)

Having rewritten the Analog Identifier, Equation (6), in decibels (dB hereafter omitted to simplify notation),

$$AID = P_{chip} - \frac{1}{2}\left(P_{R\leftarrow T} + P_{in}^{to}\right). \quad (25)$$

The smallest appreciable variation occurs when only one or even both the two powers in Equation (25) have changed by their minimum amounts, $\pm\delta P_{R\leftarrow T}$ and $\pm\delta P_{in}$, respectively. The minimum variation of AID may therefore fluctuate within the following set:

$$\left|\delta AID_{min}\right| \in \left\{\frac{\left|\delta P_{R\leftarrow T} \pm \delta P_{in}\right|}{2}, \frac{\delta P_{R\leftarrow T}}{2}, \frac{\delta P_{in}}{2}\right\}, \quad (26)$$

and, accordingly, the minimum resolution will be

$$\left|\delta AID_{min}\right| \le \frac{\delta P_{R\leftarrow T} + \delta P_{in}}{2}. \quad (27)$$

For example, a reader with $\delta P_{in} = 0.5$ dB and $\delta P_{R\leftarrow T} = 0.8$ dB will enable a resolution $|\delta AID| \le 0.65$ dB, thus better than the resolution over the backscattered power. Assuming an equal dynamic range, $\Delta\xi = 3$ dB, for all the above three metrics, then according to Equation (23), the number of detectable states of the process will be $n\left[P_{in}^{to}\right] = 6$, $n\left[P_{R\leftarrow T}\right] = 3$, and $n[AID] = 4$.

Table 2 shows some examples of the estimated overall system performance for S-tags able to sense humidity, strain, and filling level with respect to the resolution of the readers' receiver. It can be noted that a resolution of $\delta\xi < 0.5$ dB could easily guarantee the discrimination of more than 20 grades (gradations) of the process.

7. Emerging Sensing Paradigms

An emerging passive-sensing architecture considers the RFID tag as a true data-logger: physical information collected by a specific sensor is handled by a microcontroller, sampled and encoded into digital information that can be stored in the microchip's memory, and then recovered by the reader through regular RFID interrogation. These objects are usually battery assisted, and they hence act as semi-active devices. However, if the microcontroller requires very low power consumption (a few milliwatts), the energy required to drive the data acquisition may be directly harvested out of some cycles of the interrogation signal, or generated by piezo-electric energy scavengers, or by solar panels. A super-capacitor is hence required for energy storage. Examples of this class of device are the WISP [56] and the platform in [57], both of which can be integrated with general-purpose sensors. The former device codes the measured data into the ID transmitted by the tag, while the latter device is instead a battery-assisted multi-ID tag. It is capable of transmitting – when interrogated by a standard RFID reader – a proper combination of ID codes that unequivocally represents the measured value.

Table 2. Examples of the performance of S-tags.

Sensor	$\Delta\xi$ (dB)	S	$\delta\xi$ (dB)	n
Humidity [47]	12	0.3 dB/RH%	1	12
			0.5	24
			0.1	120
Strain [36]	10	0.5 dB/ε %	1	10
			0.5	20
			0.1	100
Level [27]	15	0.08 dB/mm	1	15
			0.5	30
			0.1	150

Off-the-shelf RFID ICs with augmented sensing capabilities are available nowadays [58, 59]. They include high-speed non-volatile memory (EEPROM), typically integrate an embedded temperature sensor, and provide programmable I/O ports for connecting general-purpose microcontrollers and sensors, as in [60]. These devices can be considered as a convergence point among fully passive tags, such as those described in this paper, and the autonomous sensor nodes having local computational capability. Indeed, they could be practically immune to the environmental interactions, and the onboard sensors can be moreover extremely specific. They thus could provide a possible tradeoff between superior sensing performance and cost. The electromagnetic challenge is rather small, since the sensing and communication functionalities are fully decoupled.

8. Conclusion

The applicability of RFID technology to passive sensing is now a fact, demonstrated by much independent research worldwide. Many more examples are expected to come in the next few years, stimulated by the virtuous interaction among different areas of expertise. In particular, RFID chemical sensors could have great commercial interest, thanks to the simplicity of fabrication and to the potential mass diffusion in food and pharmaceutical-control chains.

Anyway, the design of S-tags is not yet a mature discipline, since unified methodologies are still required to efficiently handle multi-physics optimization and data processing. This is a kind of short-range sensing. It is therefore expected that some methods will be borrowed from the more-assessed and mature remote-sensing background.

The sensitivity and resolution of the reader are currently the main bottlenecks of the passive S-tag technology. These critical issues are expected to be mitigated in the future generations of readers (mainly by increasing the analog-to-digital converter performance). The concurrent reduction of the chip's sensitivity will enable a close integration of this technology in general-purpose smart phones, with unpredictable applications in distributed or ubiquitous computing boosting the evolution of the Internet of Things.

At the very end, the new all-on-chip multifunction components described in Section 7, which at most require only external storage capacitors and promise high sensing accuracy, are now available. It is now paradoxically necessary to raise the question of whether or not to continue doing research on completely passive radio sensors, involving less-accurate and still-challenging analog reading. The answer is not unequivocal, and cannot be kept separate from the application fields. All those sensors *disappearing into things* (as claimed by Mark Wiser in his popular essay on "The Computer for the 21st Century" [61], e.g., for really massive and pervasive applications), require being as simple, cheap, and small as possible. Hence, the research on sensitive antennas, with a so-big physical insight, definitely keeps on making sense. For biomedical applications, completely passive radio sensors are useful as well to enable the widespread diffusion of smart disposable devices, e.g., plasters enhanced with sensing and communication functionalities. For integration with implantable devices, the possibility of avoiding batteries and additional components will simplify the biocompatibility of the radio sensor. Such an advantage overcomes the eventual drawbacks related to low resolution. Sporadic placements – for instance, in the case of precise environmental monitoring, wherein the accuracy of the measurement is the main requirement, but the reading distance is not a particular issue – will instead greatly benefit from battery- or capacitor-assisted RFID ICs. These could be a strategic choice as the short-range version of the more-complex but powerful autonomous sensor nodes.

9. References

1. D. M. Dobkin, *The RF in RFID: Passive UHF RFID in Practice*, Amsterdam, Elsevier, 2007.

2. L. Atzori, A. Iera, and G. Morabito, "The Internet of Things: A Survey," *Computer Networks*, **54**, 15, pp. 2787-2805, 2010; available at: http://www.sciencedirect.com/ science/article/pii/ S1389128610001568.

3. J. Rabaey, "The Swarm at the Edge of the Cloud – A New Perspective on Wireless," 2011 Symposium on VLSI Circuits (VLSIC), June 2011, pp. 6-8.

4. R. Bhattacharyya, C. Floerkemeier, and S. Sarma, "Low-Cost, Ubiquitous RFID-Tag-Antenna-Based Sensing," *Proceedings of the IEEE*, **98**, 9, September 2010, pp. 1593-1600.

5. B. Warneke, M. Last, B. Liebowitz, and K. Pister, "Smart Dust: Communicating with a Cubic-Millimeter Computer," *Computer*, **34**, 1, January 2001, pp. 44-51.

6. L. Theremin, "Signaling Apparatus," February 1928.

7. G. Marrocco, "The Art of UHF RFID Antenna Design: Impedance-Matching and Size-Reduction Techniques," *IEEE Antennas and Propagation Magazine*, **50**, 1, February 2008, pp. 66-79.

8. G. Marrocco, "Pervasive Electromagnetics: Sensing Paradigms by Passive RFID Technology," *IEEE Wireless Communications*, **17**, 6, December 2010, pp. 10-17.

9. EPC Radio-Frequency Identity Protocols Class-1 Generation-2 UHF RFID Protocol for Communications at 860 MHz - 960 MHz, http://www.gs1.org/gsmp/kc/epcglobal/ uhfc1g2/.

10. G. Marrocco, L. Mattioni, and C. Calabrese, "Multiport Sensor RFIDs for Wireless Passive Sensing of Objects: Basic Theory and Early Results," *IEEE Transactions on Antennas and Propagation*, **AP-56**, 8, August 2008, pp. 2691-2702.

11. G. Marrocco, "RFID Grids: Part I: Electromagnetic Theory," *IEEE Transactions on Antennas and Propagation*, **AP-59**, 3, March 2011, pp. 1019-1026.

12. S. Caizzone and G. Marrocco, "RFID Grids: Part II: Experimentations," *IEEE Transactions on Antennas and Propagation*, **AP-59**, 8, August 2011, pp. 2896-2904.

13. P. Nikitin and K. Rao, "Theory and Measurement of Backscattering from RFID Tags," *IEEE Antennas and Propagation Magazine*, **48**, 6, December 2006, pp. 212-218.

14. F. Fuschini, C. Piersanti, F. Paolazzi, and G. Falciasecca, "Analytical Approach to the Backscattering from UHF RFID Transponder," *IEEE Antennas and Wireless Propagation Letters*, **7**, 2008, pp. 33-35.

15. G. Marrocco and F. Amato, "Self-Sensing Passive RFID: From Theory to Tag Design and Experimentation," European Microwave Conference, 2009, October 2009, pp. 001-004.

16. J. Bolomey, S. Capdevila, L. Jofre, and J. Romeu, "Electromagnetic Modeling of RFID-Modulated Scattering Mechanism. Application to Tag Performance Evaluation," *Proceedings of the IEEE*, **98**, 9, September 2010, pp. 1555-1569.

17. S. Merilampi, P. Ruuskanen, T. Bjorninen, L. Ukkonen, and L. Sydan-heimo, "Printed Passive UHF RFID Tags as Wearable Strain Sensors," 2010 3rd International Symposium on Applied Sciences in Biomedical and Communication Technologies (ISABEL), November 2010, pp. 1-5.

18. J. Gao, J. Siden, and H.-E. Nilsson, "Printed Electromagnetic Coupler with an Embedded Moisture Sensor for Ordinary Passive RFID Tags," *IEEE Electron Device Letters*, 32, 12, December 2011, pp. 1767-1769.

19. C. Occhiuzzi, G. Contri, and G. Marrocco, "Design of Implanted RFID Tags for Passive Sensing of Human Body: The STENTag," *IEEE Transactions on Antennas and Propagation*, **AP-60**, 7, July 2012, pp. 3146-3154.

20. R. Bhattacharyya, C. Floerkemeier, S. Sarma, and D. Deavours, "RFID Tag Antenna Based Temperature Sensing in the Frequency Domain," 2011 IEEE International Conference on RFID (RFID), April 2011, pp. 70-77.

21. S. Caizzone, C. Occhiuzzi, and G. Marrocco, "Multi-Chip RFID Antenna Integrating Shape-Memory Alloys for Detection of Thermal Thresholds," *IEEE Transactions on Antennas and Propagation*, **AP-59**, 2011.

22. G. Marrocco, "Gain-Optimized Self-Resonant Meander Line Antennas for RFID Applications," *IEEE Antennas and Wireless Propagation Letters*, **2**, 1, 2003, pp. 302-305.

23. C. Calabrese and G. Marrocco, "Meandered-Slot Antennas for Sensor-RFID Tags," *IEEE Antennas and Wireless Propagation Letters*, **7**, 2008, pp. 5-8.

24. C. Occhiuzzi and G. Marrocco, "Electromagnetic Optimization of Passive RFID Sensor Nodes," 2012 Proceedings of the Sixth European Conference on Antennas and Propagation (EuCAP), 2012, pp. 70-77.

25. J. Robinson and Y. Rahmat-Samii, "Particle Swarm Optimization in Electromagnetics," *IEEE Transactions on Antennas and Propagation*, **AP-52**, 2, February 2004, pp. 397- 407.

26. G. Deschamps, "Impedance of an Antenna in a Conducting Medium," *IRE Transactions on Antennas and Propagation*, **AP-10**, 5, September 1962, pp. 648-650.

27. R. Bhattacharyya, C. Floerkemeier, and S. Sarma, "RFID Tag Antenna Based Sensing: Does Your Beverage Glass Need a Refill?" 2010 IEEE International Conference on RFID, April 2010, pp. 126-133.

28. H.-E. Nilsson, J. Siden, and M. Gulliksson, "An Incontinence Alarm Solution Utilizing RFID Based Sensor Technology," 2011 IEEE International Conference on RFID-Technologies and Applications (RFID-TA), September 2011, pp. 359-363.

29. S. Capdevila, L. Jofre, J. Romeu, and J. Bolomey, "Passive RFID Based Sensing," 2011 IEEE International Conference on RFID-Technologies and Applications (RFID-TA), September 2011, pp. 507-512.

30. C.-F. Huang and J.-H. Lin, "A Warning System Based on the RFID Technology for Running-Out of Injection Fluid," 2011 Annual International Conference of the IEEE Engineering in Medicine and Biology Society, September 3, 2011, pp. 2212-2215.

31. S. Capdevila, G. Roqueta, M. Guardiola, L. Jofre, J. Romeu, and J. C. Bolomey, "Water Infiltration Detection in Civil Engineering Structures Using RFID," 2012 6th European Conference on Antennas and Propagation (EUCAP), March 2012, pp. 2505-2509.

32. S. Capdevila, L. Jofre, J.-C. Bolomey, and J. Romeu, "***RFID Multi-Probe Impedance-Based Sensors," IEEE *Transactions on Instrumentation and Measurement*, **59**, 12, December 2010, pp. 3093-3101.

33. R. Suwalak, C. Phongcharoenpanich, D. Torrungrueng, and M. Krairiksh, "Determination of Dielectric Property of Construction Material Products Using a Novel RFID Sensor," *Progress In Electromagnetics Research*, **130**, 2012, pp. 601-617.

34. Z. Jiang, Z. Fu, and F. Yang, "RFID Tag Antenna Based Wireless Sensing Method for Medical Transfusion Applications," 2012 IEEE International Conference on RFID-Technologies and Applications (RFID-TA), September 2012.

35. C. Occhiuzzi and G. Marrocco, "Sensing the Human Body by Implanted RFID Tags," 2010 Proceedings of the Fourth European Conference on Antennas and Propagation (EuCAP), April 2010, pp. 1-5.

36. C. Occhiuzzi, C. Paggi, and G. Marrocco, "Passive RFID Strain-Sensor Based on Meander-Line Antennas," *IEEE Transactions on Antennas and Propagation*, **AP-59**, 12, December 2011, pp. 4836-4840.

37. R. Bhattacharyya, C. Floerkemeier, and S. Sarma, "Towards Tag Antenna Based Sensing – An RFID Displacement Sensor," 2009 IEEE International Conference on RFID, April 2009, pp. 95-102.

38. X. Yi, C. Cho, C.-H. Fang, J. Cooper, V. Lakafosis, R. Vyas, Y. Wang, R. T. Leon, and M. M. Tentzeris, "Wireless Strain and Crack Sensing Using a Folded Patch Antenna," 2012 6th European Conference on Antennas and Propagation (EUCAP), March 2012, pp. 1678-1681.

39. R. Krigslund, S. Dosen, P. Popovski, J. Dideriksen, G. Pedersen, and D. Farina, "A Novel Technology for Motion Capture Using Passive UHF RFID Tags," *IEEE Transactions on Biomedical Engineering*, 2012.

40. C. Occhiuzzi and G. Marrocco, "The RFID Technology for Neurosciences: Feasibility of Limbs' Monitoring in Sleep Diseases," *IEEE Transactions on Information Technology in Biomedicine*, **14**, 1, January 2010, pp. 37-43.

41. A. Vaz, A. Ubarretxena, I. Zalbide, D. Pardo, H. Solar, A. Garcia-Alonso, and R. Berenguer, "Full Passive UHF Tag with a Temperature Sensor Suitable for Human Body Temperature Monitoring," *IEEE Transactions on Circuits and Systems II: Express Briefs*, **57**, 2, February 2010, pp. 95-99.

42. S. Caizzone, C. Occhiuzzi, and G. Marrocco, "Multi-Chip RFID Antenna Integrating Shape-Memory Alloys for Detection of Thermal Thresholds," *IEEE Transactions on Antennas and Propagation*, **AP-59**, 7, July 2011, pp. 2488-2494.

43. J. Virtanen, L. Ukkonen, T. Bjorninen, A. Elsherbeni, and L. Sydanheimo, "Inkjet-Printed Humidity Sensor for Passive UHF RFID Systems," *IEEE Transactions on Instrumentation and Measurement*, **60**, 8, August 2011, pp. 2768-2777.

44. L. Yang, R. Zhang, D. Staiculescu, C. Wong, and M. Tentzeris, "A Novel Conformal RFID-Enabled Module Utilizing Inkjet-Printed Antennas and Carbon Nanotubes for Gas-Detection Applications," *IEEE Antennas and Wireless Propagation Letters*, **8**, 2009, pp. 653-656.

45. C. Occhiuzzi, A. Rida, G. Marrocco, and M. Tentzeris, "RFID Passive Gas Sensor Integrating Carbon Nanotubes," *IEEE Transactions on Microwave Theory and Techniques*, 2011.

46. L. Mattioni and G. Marrocco, "Blade: A Broadband Loaded Antenna Designer," *IEEE Antennas and Propagation Magazine*, **48**, 5, October 2006, pp. 120-129.

47. S. Johan, X. Zeng, T. Unander, A. Koptyug, and H.-E. Nilsson, "Remote Moisture Sensing Utilizing Ordinary RFID Tags," 2007 IEEE Sensors, October 2007, pp. 308-311.

48. S. Manzari, C. Occhiuzzi, S. Nawale, A. Catini, C. Di Natale, and G. Marrocco, "Humidity Sensing by Polymer-Loaded UHF RFID Antennas," IEEE Sensors, 2012.

49. J. Virtanen, L. Ukkonen, T. Bjoandrninen, A. Z. Elsherbeni, and L. Sydaandnheimo, "Inkjet-Printed Humidity Sensor for Passive UHF RFID Systems," *IEEE Transactions on Instrumentation and Measurement*, 2011.

50. J. Virtanen, L. Ukkonen, T. Bjorninen, L. Sydanheimo, and A. Elsherbeni, "Temperature Sensor Tag for Passive UHF RFID Systems," 2011 IEEE Sensors Applications Symposium (SAS), February 2011, pp. 312-317.

51. A. Babar, S. Manzari, L. Sydanheimo, A. Elsherbeni, and L. Ukkonen, "Passive UHF RFID Tag for Heat Sensing Applications," *IEEE Transactions on Antennas and Propagation*, **AP-60**, 9, September 2012, pp. 4056-4064.

52. Q. Qiao, F. Yang, and A. Elsherbeni, "Read Range and Sensitivity Study of RFID Temperature Sensors," 2012 IEEE International Symposium on Antennas and Propagation, July 2012, pp. 1-2.

53. C. Occhiuzzi, S. Cippitelli, and G. Marrocco, "Modeling, Design and Experimentation of Wearable RFID Sensor Tag," *IEEE Transactions on Antennas and Propagation*, **AP-58**, 8, pp. 2490-2498, August 2010, pp. 2490-2498.

54. M. Philipose, J. Smith, B. Jiang, A. Mamishev, S. Roy, and K. Sundara-Rajan, "Battery-Free Wireless Identification and Sensing," *IEEE Pervasive Computing*, **4**, 1, January-March 2005, pp. 37- 45.

55. R. Bhattacharyya, C. Floerkemeier, and S. Sarma, "RFID Tag Antenna Based Temperature Sensing," 2010 IEEE International Conference on RFID, April 2010, pp. 8-15.

56. A. Sample, D. Yeager, P. Powledge, and J. Smith, "Design of a Passively-Powered, Programmable Sensing Platform for UHF RFID Systems," 2007 IEEE International Conference on RFID, March 2007, pp. 149-156.

57. L. Catarinucci, R. Colella, and L. Tarricone, "A Cost-Effective UHF RFID Tag for Transmission of Generic Sensor Data in Wireless Sensor Networks," *IEEE Transactions on Microwave Theory and Techniques*, **57**, 5, May 2009, pp. 1291-1296.

58. EM 4325, available at www.emmicroelectronic.com.

59. NXP Ucode I2C, available at www.nxp.com.

60. T. Unander, J. Siden, and H.-E. Nilsson, "Designing of RFID-Based Sensor Solution for Packaging Surveillance Applications," *IEEE Sensors Journal*, **11**, 11, November 2011, pp. 3009-3018.

61. M. Weiser, "The Computer for the 21st Century," *Scientific American*, September 1991, pp. 933-940.

Introducing the Feature Article Authors

Cecilia Occhiuzzi received the MSc in Medical Engineering and the PhD in Electromagnetics from the University of Rome "Tor Vergata," in 2008 and 2011, respectively. Currently, she is a Research Assistant in the University of Rome "Tor Vergata," with interests in wireless health monitoring by means of wearable and implantable radio-frequency identification techniques. In 2008, she was with the School of Engineering, University of Warwick, Warwick, UK, as a postgraduate student, involved with design and implementation of wireless surface-acoustic-wave (SAW) sensors. In 2010, she was a Visiting Researcher with the Georgia Institute of Technology, Atlanta. Her research was mainly focused on the design of passive RFID sensors for structural health monitoring and gas detection by means of CNT-based tags. She holds two patents on sensor RFID systems.

Stefano Caizzone received the MSc in Telecommunications Engineering from the University of Rome "Tor Vergata" in 2009, and he is currently working part-time toward the PhD. His main research interests concern small antennas for RFID and navigation, antenna arrays and grids with enhanced sensing capabilities. He is now with the Antenna group of the Institute of Communications and Navigation of the German Aerospace Center (DLR), Wessling, Germany, where he is responsible for the development of innovative miniaturized antennas.

Gaetano Marrocco was born in Teramo, Italy, in 1969. He received the Laurea in Electronic Engineering (Laurea cum Laude and Academic Honour) and the PhD in Applied Electromagnetics from the University of L'Aquila, Italy, in 1994 and 1998, respectively. Since 1997, he has been a Researcher at the University of Rome "TorVergata," Rome, Italy. There, he currently teaches "Electromagnetic Technology for Wireless Systems and Medical Radio-Systems," manages the Pervasive Electromagnetics Lab, and is advisor in the Geo-Information PhD program. In October 2010, he achieved the position of Associate Professor of Electromagnetics.

In 1994, he was at the University of Illinois at Urbana-Champain as a Postgraduate Student. In 1999, he was a Visiting Researcher at the Imperial College in London, UK. In 2008 he joined the PhD program of the University of Grenoble, France. His research is mainly directed toward the modeling and design of broadband and ultra-wideband (UWB) antennas and arrays, as well as of sensor-oriented miniaturized antennas for biomedicine, aeronautics and radio-frequency identification (RFID). Prof. Marrocco has been involved in several space, avionic, naval, and vehicular programs of the European Space Agency, NATO, the Italian Space Agency, and the Italian Navy, on the analysis and the design of non-conventional antennas and systems over platforms. He has submitted eight patents on broadband naval antennas and structural arrays, and on sensor RFID systems.

He currently serves as Associate Editor of the *IEEE Antennas and Wireless Propagation Letters*, Vice Chair of the Italian delegation for URSI Commission D, and as a member of the Technical Program Committee of IEEE RFID, IEEE IMS, and ISABEL. In 2008, he was the General Chair of the first Italian multidisciplinary scientific workshop on RFID: RFIDays-2008: Emerging Technology for Radiofrequency Identification. He was the co-Chair of the RFIDays-2010 International Workshop in Finland, and Chair of the Local Committee of the V European Conference on Antennas and Propagation and TCP chair of the 2012 IEEE-RFID TA in Nice, France.